

# Nonthermal Emission from Star-Forming Galaxies

Yoel Rephaeli and Massimo Persic

**Abstract** The detections of high-energy  $\gamma$ -ray emission from the nearby starburst galaxies M 82 & NGC 253, and other local group galaxies, broaden our knowledge of star-driven nonthermal processes and phenomena in non-AGN star-forming galaxies. We review basic aspects of the related processes and their modeling in starburst galaxies. Since these processes involve both energetic electrons and protons accelerated by SN shocks, their respective radiative yields can be used to explore the SN-particle-radiation connection. Specifically, the relation between SN activity, energetic particles, and their radiative yields, is assessed through respective measures of the particle energy density in several star-forming galaxies. The deduced energy densities range from  $\mathcal{O}(10^{-1})$  eV cm $^{-3}$  in very quiet environments to  $\mathcal{O}(10^2)$  eV cm $^{-3}$  in regions with very high star-formation rates.

## 1 Introduction

High star formation (SF) and supernova (SN) rates in starburst (SB) galaxies (SBGs) boost the density of energetic nonthermal particles, whose main constituents are protons and electrons. Coulomb, synchrotron and Compton energy losses by the electrons, and the decay of pions following their production in energetic proton interactions with protons in the ambient gas, result in emission over the full electromagnetic spectrum, from radio to very high-energy (VHE,  $\geq 100$  GeV)  $\gamma$ -rays. The

---

Yoel Rephaeli  
School of Physics and Astronomy, Tel Aviv University, Tel Aviv, 69978, Israel  
and  
Center for Astrophysics and Space Sciences, University of California, San Diego, La Jolla, CA 92093-0424, USA, e-mail: yoelr@wise.tau.ac.il

Massimo Persic  
INAF/Osservatorio Astronomico di Trieste and INFN-Trieste, via G.B.Tiepolo 11, I-34143 Trieste, Italy e-mail: persic@oats.inaf.it

relatively high intensity emission in SBGs, as compared with emission from ‘normal’ star-forming galaxies (SFGs), makes nearby members of this class the most likely non-AGN targets for  $\gamma$ -ray telescopes, such as *Fermi* and the (Cherenkov arrays) H.E.S.S., MAGIC, and VERITAS.

Interest in  $\gamma$ -ray emission from SFGs clearly stems from the prospects for improved understanding of the origin and propagation mode of energetic electrons and protons and their coupling to interstellar media. This interest has been enhanced by recent detections of the two nearby SBGs M82 & NGC253 by *Fermi* (Abdo et al. 2010a) and, respectively, by H.E.S.S. (Acciari et al. 2009) and VERITAS (Acero et al. 2009). M31, the closest normal spiral galaxy, was also detected by *Fermi* (Abdo et al. 2010b).

A realistic estimate of the expected  $\gamma$ -ray emission requires a detailed account of all relevant energy loss processes of energetic electrons and protons as they move out from the central SB source region into the outer galactic disk. Calculations of the predicted X- $\gamma$ -ray spectra of nearby galaxies were made long ago with varying degree of detail (e.g., Goldshmidt & Rephaeli 1995, Paglione et al. 1996, Romero & Torres 2003, Domingo-Santamaría & Torres 2005). A more quantitative numerical approach was initiated by Arieli & Rephaeli (2007, unpublished), who used a modified version of the GALPROP code (Moskalenko & Strong 1998, Moskalenko et al. 2003) to solve the Fokker-Planck diffusion-convection equation (e.g., Lerche & Schlickeiser 1982) in 3D with given source distribution and boundary conditions for electrons and protons. This numerical treatment was implemented to predict the high-energy spectra of the two nearby galaxies M82 (Persic, Rephaeli, & Arieli 2008, hereafter PRA) and NGC253 (Rephaeli, Arieli, & Persic 2010, hereafter RAP). The predictions made in these papers agree well with observations made with *Fermi* and TeV arrays, as will be discussed in the next section.

Particle acceleration and propagation in galactic environments are largely similar in all SFGs. What mainly distinguishes a SBG from a normal SFG is the dominance of a relatively small central region of intense star formation activity. The overall validity of the numerical treatments of the two nearby SBGs provides a solid basis for generalizing the model to SFGs in general.

We briefly review the calculation of steady-state particle spectra and their predicted radiative spectra for the above two nearby SBGs, and discuss similar calculations for conditions in a SFG. The particle energy density can be determined in several different ways. In order to assess and gauge the SN-energetic particle connection we compare estimates of the energetic proton (which dominate the) energy density in SFGs by three different methods, finding overall agreement, which provides further evidence for the validity of the basic approach.

## 2 Particle and Radiation Spectra in Starburst Galaxies

Acceleration in SN shocks by the first-order Fermi process yields a power-law distribution with index  $q \geq 2$  (e.g., Protheroe & Clay 2004) in a very wide energy range,

from a value close to the mean thermal energy of the gas particles (in non-relativistic shocks) to a very high value ( $\geq 10^{14}$  eV). The accelerated proton-to-electron (p/e) density ratio,  $N_p/N_e$ , in the source (either the SB or the full disk) region can be calculated assuming charge neutrality (Bell 1978, Schlickeiser 2002). This ratio reaches its maximum value,  $(m_p/m_e)^{(q-1)/2}$  (for  $q > 1$ ;  $m_e$  and  $m_p$  are the electron and proton masses), over most of the relevant range of particle energies,  $E > 1$  GeV. (For the dependence of this ratio on particle energy, and more discussion on this and other relevant physical processes, see PRA and references therein.)

The electron density in the source region,  $N_e$ , is inferred from radio measurements (of the same region); by adopting the theoretically expected expression  $N_p/N_e = (m_p/m_e)^{(q-1)/2}$ , the proton density  $N_p$  can be deduced. The fit to the radio data provides both the normalization of the electron spectrum and the *actual* value of  $q$ , which is found to be somewhat larger than 2, even in the central SB region. In this procedure the electron population is composed of both primary and secondary electrons, with the latter self-consistently determined by accounting for the pion yield of energetic protons with protons in the gas. We note that the theoretically predicted value of the density ratio is valid in the source region, where energy equipartition is more likely to be attained since the relevant processes couple particles and fields more effectively than in the rest of galactic disk.

The particle spectral distributions evolve differently as they propagate out from their acceleration region. Typically, the electron spectrum is most directly deduced from measurements of synchrotron radio emission. The inferred spectrum can be related to the source spectrum through a solution of the kinetic equation describing the propagation modes and energy losses by electrons and protons as they move out from their acceleration region. A very useful detailed description of the time-dependent spectro-spatial distribution of protons, diffusing out of a region with a discrete population of acceleration sites, was recently given by Torres et al. (2012). This study elucidates the explicit dependence of the distribution on distance from the acceleration site, energy loss time, and the diffusion coefficient. It also follows the temporal evolution of the distribution towards a steady state.

Since the estimated duration of a SB phase is  $\sim 10^8$  yr, a timescale which is much longer than any of the relevant energy loss or propagation timescales for electrons and protons, in (essentially) all treatments a steady state is assumed to be attained. Since the calculation of particle steady-state spectra requires inclusion of all the important energy loss mechanisms and modes of propagation, the treatment is necessarily numerical. We have employed the code of Arieli & Rephaeli (2007), which is based on a modified version of the GALPROP code (Moskalenko & Strong 1998, Moskalenko et al. 2003), to solve the kinetic equation for  $N_i(\gamma, R, z)$ , where  $i = e, p$ ,  $\gamma$  is the Lorentz factor, and  $R$  and  $z$  are the 2D spatial radius and the coordinate perpendicular to the galactic plane. The exact Fokker-Planck diffusion-convection equation (e.g., Lerche & Schlickeiser 1982) was solved in 3D with given source distribution and boundary conditions for electrons and protons. In addition to diffusion with an energy dependent coefficient, particles are assumed to be convected by a galactic wind with spatially varying velocity.

The dominant energy losses of high-energy electrons are synchrotron emission and Compton scattering by the FIR and optical radiation fields; these processes (obviously) depend on the mean strength of the magnetic field,  $B$ , and the energy density of the radiation fields, respectively. At energies below few hundred MeV, electrons lose energy mostly by Coulomb interactions with gas particles. At low energies proton losses are dominated by Coulomb interactions with gas particles. Protons with kinetic energy above the (range of) pion masses ( $\sim 140$  MeV) lose energy mainly through interactions with ambient protons, yielding neutral ( $\pi^0$ ) and charged ( $\pi^\pm$ ) pions. Neutral pions decay into photons, while decays of  $\pi^\pm$  result in energetic  $e^\pm$  and neutrinos. The proton and (total) electron components are coupled through the production of secondary electrons in  $\pi^-$  decay (following their creation in  $pp$  interactions).

Measured synchrotron radio spectra provide the critically important information on the particle spectra and their overall normalization: Fitting the predicted radio emission to measurements fixes normalization of the steady state electron and - based on a theoretical prediction - proton energy distributions. From these measurements alone the electron density and mean magnetic field cannot be separately determined. To do so it is usually assumed that particle and magnetic field energy densities are equipartitioned. In our numerical treatment this approach necessitates an iterative procedure to solve for  $N_e$ ,  $N_p$ , and the field strength at the center,  $B_0$ , given a measured value of the radio flux.

Particles diffuse and are convected out of their source region. Diffusion is likely to be random walk against magnetic field inhomogeneities, with an estimated value of  $\sim 3 \times 10^{28}$  cm<sup>2</sup>/s for the central diffusion coefficient. Convection is by galactic wind with a typical velocity of  $\sim 500$  km s<sup>-1</sup> (Strickland et al. 1997) in the source region. Based on Galactic cosmic-ray MHD wind models, we assume that the convection velocity increases linearly with distance from the disk plane (e.g. Zirakashvili et al. 1996).

The other quantities needed to calculate the steady state distributions of electrons and protons are the densities of neutral and ionized gas in the central SB region and throughout the disk, the central value of the (mean) magnetic field and its spatial profile across the disk, and energy densities of ambient radiation fields (including the CMB). As discussed in PRA, it is assumed that magnetic flux is conserved in the IS ionized gas, so that the mean strength of the field can be related to the local ionized gas density,  $n_e$ , using the scaling  $B \propto n_e^{2/3}$  (Rephaeli 1988). If instead energy equipartition is assumed, and the magnetic energy density is scaled to the thermal gas energy density, then the proportionality relation is  $B \propto n_e^{1/2}$ . In our work we have taken the ionized gas density profile to be  $n_e \propto \exp(-z/z_0)/(1 + (R/R_0)^2)$ , typically with  $R_0 = 1.5$  kpc, and  $z_0 = 0.5$  kpc (as deduced for NGC 253 by Strickland et al. 2002).

Given the measured radio fluxes from the central and full disk regions of the two nearby SBGs M82 and NGC253, shown in Figure 1 for the latter galaxy, and values of all the above quantities, the steady state particle spectra and their radiative yields were calculated using the modified GALPROP code. Here we present the results of

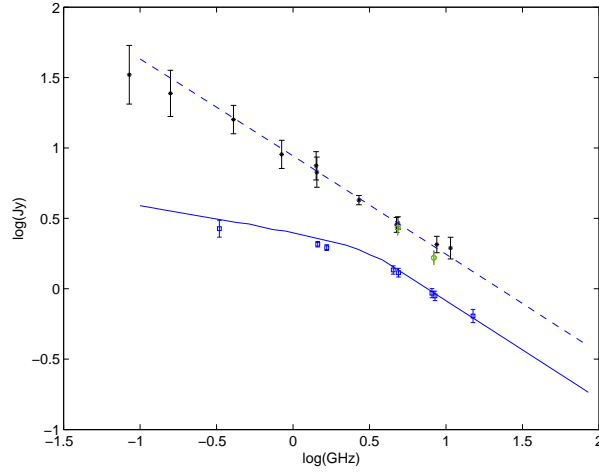


**Fig. 1** Spectral fits to radio measurements of the SB and entire disk regions of NGC 253 (RAP). The solid line is a fit to the emission from the SB region; the dashed line is a fit to the emission from the entire disk. Data are from Klein et al. (1983, black dots), Carilli (1996, blue squares), and Heesen et al. (2008, green circles).

this work; more details on the method and values of the input parameters can be found in PRA and RAP.

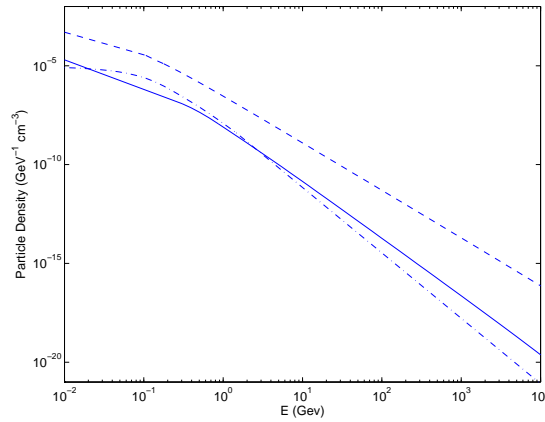


**Fig. 2** Primary proton (dashed line), primary electron (solid line), and secondary electron (dashed-dotted line) spectral steady state density distributions in the central SB region NGC 253 (RAP).

The high-energy photon spectra of NGC253 are shown in Figure 3 (from RAP). Emission levels depend mostly on values of the proton to electron ratio in the source region, on the magnetic field, gas density, and their spatial profiles. The basic normalization of the electron density is provided by the measured radio emission in

the source region; the variation of the electron spectrum across the disk is largely determined by synchrotron losses. Uncertainty in the estimated level of emission is largely due to the steep dependence of the electron density on the field. As argued by RAP, the central value of the (mean) magnetic field is unlikely to be appreciably higher than the value deduced in N253 (and also in M82),  $B_0 \sim 200 \mu\text{G}$ . A lower field value would result in a reduced proton density and a lower rate of  $\pi^0$  decays. For a given radio flux the electron density would have to be correspondingly higher, resulting in higher bremsstrahlung and Compton yields, roughly compensating for the lower level of hadronic emission. Emission from  $\pi^0$  decay depends linearly on the ambient proton density in the central disk region.

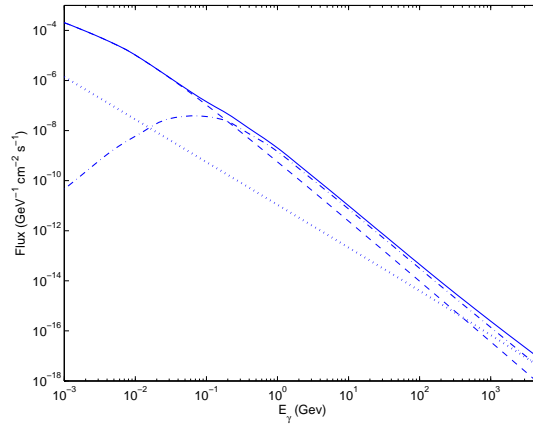


**Fig. 3** High-energy emission from the disk of NGC 253. Radiative yields are from Compton scattering off the FIR radiation field (dotted line), electron bremsstrahlung off ambient protons (dashed line),  $\pi^0$  decay (dashed-dotted line), and their sum (solid line).

Detailed modeling of high-energy emission from M82 by PRA preceded its detection by VERITAS (Acciari et al. 2009) and *Fermi* (Abdo et al. 2010a). These observations are shown in Figure 4 (from Abdo et al. 2010a), together with theoretical predictions including that of PRA. The detected flux level agrees well with that predicted by PRA and by de Cea et al. 2009. Results from our similar treatment of the steady-state particle and radiation spectra of NGC253 were presented in RAP. The estimated high energy fluxes for this galaxy (RPA, Paglione et al. 1996, Domingo-Santamaria & Torres 2005) were also in the range measured by *Fermi* (Abdo et al. 2010a), and - in the TeV region - by the HESS telescope (Acero et al. 2009), given the substantial observational and modeling uncertainties. These observational results and predicted spectra are shown in Figure 5 (adopted from Abdo et al. 2010a); our integrated spectrum and estimated  $1\sigma$  uncertainty region are marked by the dashed blue lines (inserted into the original figure). These two SBGs are the only extragalactic non-AGN sources that were detected at both GeV and TeV energies. The FIR luminosities of these galaxies are at or somewhat below the nominal level for SBGs; clearly, their apparent high brightness is due to their proximity.

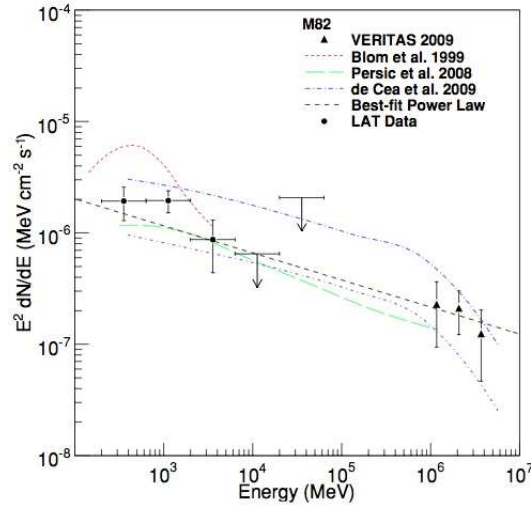


**Fig. 4** High-energy emission from M82. VERITAS (Acciari et al. 2009) and *Fermi* measurements are shown together with predicted spectra. Figure is reproduced from Abdo et al. (2010a).

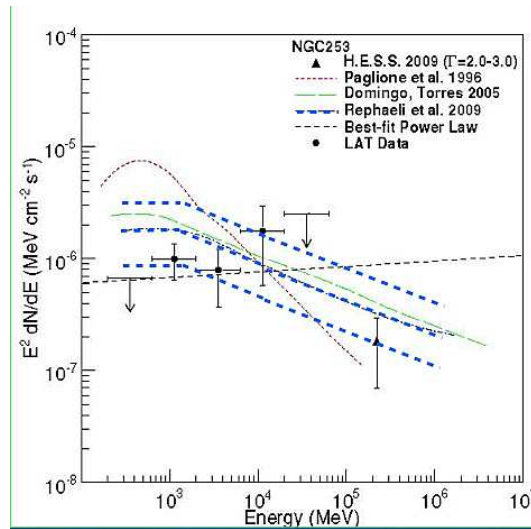


**Fig. 5** High-energy emission from the disk of NGC253. *Fermi* and H.E.S.S measurements are shown together with predicted spectra. The figure is reproduced from Abdo et al. (2010b); the added dashed blue lines show our predicted spectrum with the estimated range of  $1\sigma$  uncertainty.

A few other local and nearby galaxies were also detected at high energies: LMC (Abdo et al. 2010c), SMC (Abdo et al. 2010d), Andromeda (M31; Abdo et al. 2010b), and the composite Sy2/SB galaxies NGC 1068 and NGC 4945 (Lenain et al. 2010). The emission in these galaxies is mostly hadronic  $\gamma$ -ray emission, except for

NGC 1068 where emission from the active nucleus may be dominant. Among galaxies whose detected high energy emission is powered by stellar activity, Arp 220 has the highest SFR in the local universe, yet an attempt to detect it by MAGIC (Albert et al. 2007) was not successful due to its relatively large distance.

### 3 Estimates of Cosmic-Ray Energy Density

Active star formation in galaxies leads to acceleration of protons and electrons via the Fermi-I diffusive shock acceleration mechanism in SN remnants. Under equilibrium conditions in a galaxy, a minimum-energy configuration of the magnetic field and the energetic particles may be attained. Energy densities of particles and magnetic fields may then be in approximate equipartition, implying that the energetic proton energy density,  $U_p$ , can be deduced from the detected level of synchrotron radio emission. In this *radio-based* approach  $U_p$  can be estimated if the source size, distance, radio flux, and radio spectral index are known.

In a  *$\gamma$ -based* approach,  $U_p$  can be obtained from the measured GeV-TeV spectral flux, which is mostly due to p-p interactions, as described the previous section. Only recently have such measurements become possible, at present only for 10 sources.

In the *SN method*, with an assumed fraction of SN kinetic energy that is channeled into particle acceleration,  $U_p$  can be estimated if the size of the star-forming region and SN rate are known, as well as an estimate for the proton residence timescale from the presence (or absence) of a galactic wind emanating from the star-forming region. This timescale is largely determined by the advection timescale ( $\sim 10^5$ yr) in SBGs, and by the  $\pi^0$ -decay timescale ( $\sim 10^7$ yr) in low-SFR (quiescent) galaxies.

Expanding on our previous work (Persic & Rephaeli 2010), we show that the three methods give consistent results for  $U_p$  for a sample of 10 galaxies with widely varying levels of star formation activity, from very quiescent to extreme SBs. These are the only galaxies of their kind for which  $\gamma$ -ray data, in addition to radio data and SN rates, are available (see Table 1).

#### 3.1 Particles and magnetic field

The population of NT electrons consists of primary (directly accelerated) and secondary (produced via  $\pi^\pm$  decays) electrons. While the exact form of the steady-state electron energy spectrum is not a single power law, at high energies the flattening of the spectrum due to Coulomb losses can be ignored, justifying the use of the approximate single power-law form. The combined (primary plus secondary) electron spectral density distribution is then

$$N_e(\gamma) = N_{e,0} (1 + \chi) \gamma^{-q}, \quad (1)$$



**Table 1** Star-forming galaxies: the data.

Object	$D_L^{[1]}$ (Mpc)	$r_s^{[2]}$ (kpc)	$f_{1\text{GHz}}^{[3]}$ (Jy)	$\alpha_{\text{NT}}^{[4]}$	$n_{e,\text{th}}^{[5]}$ ( $\text{cm}^{-3}$ )	$L_{\text{TIR}}^{[6]}$ (erg/s)	SFR <sup>[7]</sup> ( $M_\odot/\text{yr}$ )	$v_{\text{SN}}^{[8]}$ ( $\text{yr}^{-1}$ )	$M_{\text{gas}}^{[9]}$ ( $M_\odot$ )	$L_\gamma^{[10]}$ (erg/s)	Notes
Arp 220	74.7	0.25	0.3	0.65	300	45.75	253	3.5	$9.24^{+0.10}_{-0.11}$	$< 42.25$	SB
M 82	3.4	0.23	10.0	0.71	200	44.26	8.2	0.25	$9.37^{+0.09}_{-0.14}$	$40.21^{+0.10}_{-0.13}$	SB
NGC 253	2.5	0.20	5.6	0.75	400	44.23	7.7	0.12	$9.20^{+0.10}_{-0.11}$	$39.76^{+0.14}_{-0.19}$	SB
Milky Way	–	4.4	–	–	0.01	43.75	2.5	0.02	$9.81^{+0.12}_{-0.16}$	$38.91^{+0.12}_{-0.15}$	quiescent
M 31	0.78	4.5	4.0	0.88	0.01	42.98	0.43	0.01	$9.88^{+0.11}_{-0.15}$	$38.66^{+0.09}_{-0.10}$	quiescent
M 33	0.85	2.79	3.30	0.95	0.03	42.68	0.22	0.003	$9.35^{+0.13}_{-0.19}$	$< 38.54$	quiescent
LMC	0.049	2.4	285.0	0.84	0.01	42.45	0.13	0.002	$8.86^{+0.12}_{-0.18}$	$37.67^{+0.05}_{-0.05}$	quiescent
SMC	0.061	1.53	45.3	0.85	0.01	41.45	0.01	0.001	$8.66^{+0.03}_{-0.06}$	$37.04^{+0.11}_{-0.14}$	quiescent
NGC 4945	3.7	0.22	5.5	0.57	300	44.02	4.7	0.1-0.5	$9.64^{+0.10}_{-0.40}$	$40.30^{+0.12}_{-0.16}$	SB+Sy2
NGC 1068	16.7	1.18	6.6	0.75	300	45.05	50	0.2-0.4	$9.71^{+0.11}_{-0.19}$	$41.32^{+0.15}_{-0.23}$	SB+Sy2

<sup>[1]</sup>Distance (from Ackermann et al. 2012).

<sup>[2]</sup>Effective radius of star-forming region. See text. Data are from Persic & Rephaeli 2010 and refs. therein (Arp 220, M 82, NGC 253), Beck & Gräve 1982 (M 31), Tabatabaei et al. 2007 (M 33), Weinberg & Nikolaev 2001 (LMC), Wilke et al. 2003 (SMC), Moorwood & Oliva 1994 (NGC 4945), Spinoglio et al. 2005 (NGC 1068).

<sup>[3]</sup>1 GHz flux density. Data are from Persic & Rephaeli 2010 and refs. therein (Arp 220, M 82, NGC 253), Beck & Gräve 1982 (M 31), Tabatabaei et al. 2007 (M 33), Klein et al. 1989 (LMC), Haynes et al. 1991 (SMC), Elmouttie et al. 1997 (NGC 4945), Kühn et al. 1981 (NGC 1068).

<sup>[4]</sup>Non-thermal spectral radio index. Data are from Persic & Rephaeli 2010 and refs. therein (Arp 220, M 82, NGC 253), Beck & Gräve 1982 (M 31), Tabatabaei et al. 2007 (M 33), Klein et al. 1989 (LMC), Haynes et al. 1991 (SMC), Elmouttie et al. 1997 (NGC 4945), Kühn et al. 1981 (NGC 1068).

<sup>[5]</sup>Thermal electron density. Data are from Roy et al. 2010 (Arp 220), Petuchowski et al. 1994 (M 82), Kewley et al. 2000 and Corral et al. 1994 (NGC 253), Cox 2005 (Milky Way), Beck 2000 (M 31), Tabatabaei et al. 2008 (M 33), Points et al. 2001 (LMC), Sasaki et al. 2002 (SMC), Spoon et al. 2000 (NGC 4945), Kewley et al. 2000 (NGC 1068).

<sup>[6]</sup>Total IR [i.e., (8 – 1000)  $\mu\text{m}$ ] luminosity, in log (from Ackermann et al. 2012).

<sup>[7]</sup>Star formation rate, from  $\text{SFR} = L_{\text{IR}} / (2.2 \times 10^{43} \text{ erg/s})$  (Kennicutt 1998).

<sup>[8]</sup>Core-collapse SN rate. Data are from Persic & Rephaeli 2010 and references therein (Arp 220, M 82, NGC 253), Diehl et al. 2006 (Milky Way), van den Bergh & Tammann 1991 (M 31, M 33, SMC, LMC; see also Pavlidou & Fields 2001), Lenain et al. 2010 and references therein (NGC 4945, NGC 1068). For NGC 1068 we also computed an upper limit to the SN rate ( $v_{\text{SN}} \leq 0.39$ ) using Mannucci et al.'s (2003) formula  $v_{\text{SN}} = (2.4 \pm 0.1) \times 10^{-2} [L_{\text{FIR}} / (10^{10} L_\odot)] \text{yr}^{-1}$ , being  $f_{\text{FIR}} = 1.26 \times 10^{-11} (2.58 f_{60} + f_{100}) \text{erg cm}^{-2} \text{s}^{-1}$  (see Helou et al. 1988) with  $f_{60} \simeq 190 \text{ Jy}$  and  $f_{100} \simeq 277 \text{ Jy}$ .

<sup>[9]</sup>Gas mass (neutral plus molecular hydrogen:  $M_{\text{HI}} + M_{\text{H}_2}$ ), in log. Data are from: Torres 2004 for Arp 220; Abdo et al. 2010a for M 82, NGC 253, and the Milky Way; Abdo et al. 2010b for M 31 and M 33; Abdo et al. 2010c for the LMC; Abdo et al. 2010d for the SMC; and Lenain et al. 2010 for NGC 4945 and NGC 1068.

<sup>[10]</sup>High-energy (>100 MeV)  $\gamma$ -ray luminosity, in log (from Ackermann et al. 2012).

where the electron Lorentz factor  $\gamma$  is in the range  $\gamma_1 \leq \gamma \leq \gamma_2$ ,  $N_{e,0}$  is a normalization factor of the primary electrons,  $\chi$  is the secondary-to-primary electron ratio, and  $q \geq 2$  is the spectral index. Ignoring the contribution of low-energy electrons with  $\gamma < \gamma_1$ , the electron energy density is  $U_e = N_{e,0} (1 + \chi) m_e c^2 \int_{\gamma_1}^{\gamma_2} \gamma^{1-q} d\gamma$ , where  $\gamma_2$  is an upper cutoff whose exact value is irrelevant in the limit of interest,  $\gamma_2 \gg \gamma_1$ . For  $q > 2$  and  $\gamma_2 \gg \gamma_1$ ,

$$U_e \simeq N_{e,0} (1 + \chi) m_e c^2 \gamma_1^{2-q} / (q - 2). \quad (2)$$

For a population of electrons (specified by Eq. 1) traversing a homogeneous magnetic field of strength  $B$  in a region with (a spherically equivalent) radius  $r_s$  located at a distance  $d$ , standard synchrotron relations yield

$$N_{e,0} (1 + \chi) = 5.72 \times 10^{-15} \psi a(q)^{-1} B^{-\frac{q+1}{2}} 250^{\frac{q-1}{2}} \quad (3)$$

where the scaled flux is  $f_{1\text{GHz}}$  Jy,  $a(q)$  is defined and tabulated in, e.g., Tucker (1975), and  $\psi \equiv \left(\frac{r_s}{0.1 \text{ kpc}}\right)^{-3} \left(\frac{d}{\text{Mpc}}\right)^2 \left(\frac{f_{1\text{GHz}}}{\text{Jy}}\right)$ . Use of Eq.(2) then yields

$$U_e \simeq \frac{2.96}{(1 + \chi)} \times 10^{-22} 250^{\frac{q}{2}} \psi \frac{\gamma_1^{-q+2}}{(q-2) a(q)} B^{-\frac{q+1}{2}}. \quad (4)$$

In order to compute  $U_e$  from Eq.(4) we need to specify  $\gamma_1$  and  $B$ . To do so we make the following assumptions:

(i) The low-energy limit of the electron power-law spectrum,  $\gamma_1$ , marks the transition (for decreasing energy) from Coulomb (Rephaeli 1979) to synchrotron losses. For an electron of energy  $\gamma$ , the synchrotron loss rate is

$$\left(\frac{d\gamma}{dt}\right)_{\text{syn}} = -1.30 \times 10^{-21} \gamma^2 \left(\frac{B}{\mu\text{G}}\right)^2 \text{ s}^{-1} \quad (5)$$

whereas the Coulomb loss rate is

$$\left(\frac{d\gamma}{dt}\right)_{\text{coul}} = -1.2 \times 10^{-12} n_{e,\text{th}} \left[1.0 + \frac{\ln(\gamma/n_{e,\text{th}})}{75}\right] \text{ s}^{-1}. \quad (6)$$

(Rephaeli 1979). We then simply assume that electrons lose energy via Coulomb scattering for  $\gamma < \gamma_1$  and via synchrotron cooling for  $\gamma > \gamma_1$ .

(ii) The particle energy density is in equipartition with that of the magnetic field,  $U_p + U_e = B^2/8\pi$ . In terms of the p/e energy density ratio,  $\kappa$ , the equipartition condition is  $U_p [1 + (1 + \chi)/\kappa] = B^2/8\pi$ , so that

$$B = \left[ \frac{7.44 \times 10^{-21}}{1 + \chi} \left[1 + \frac{\kappa}{1 + \chi}\right] \frac{\gamma_1^{2-q} 250^{q/2} \psi}{(q-2) a(q)} \right]^{\frac{2}{5+q}}. \quad (7)$$

Inserting Eq.(7) into Eq.(5) we get  $(\frac{d\gamma}{dt})_{\text{syn}} \propto \gamma_1^{2(9-q)/(5+q)}$ . Once the value of  $n_{\text{e,th}}$  is specified (see Table 1), by equating Eqs.(5, 6) we deduce  $\gamma_1$ .

The secondary-to-primary electron ratio  $\chi$ , which appears in Eq.(7), depends on the injection p/e number ratio,  $r_{p/e} = (m_p/m_e)^{(q_{\text{inj}}-1)/2}$ , and on the gas optical thickness to p-p interactions. Given the branching ratios in p-p collisions, only a third of these collisions produce electrons. The mean free path of CR protons due to p-p interactions in a medium of density  $n_p$  is  $\lambda_{\text{pp}} = (\sigma_{\text{pp}} n_p)^{-1}$ ; for protons with kinetic energy  $T \sim \text{few TeV}$  the cross section is  $\sigma_{\text{pp}} \simeq 50 \text{ mb} = 5 \times 10^{-26} \text{ cm}^2$  (Baltrusaitis et al. 1984). For a typical SB ambient gas density  $n_p \simeq 150 \text{ cm}^{-3}$ ,  $\lambda_{\text{pp}} \sim 43 \text{ kpc}$ . The probability for a single CR proton to undergo a pp interaction in its 3D random walk through a region of radius  $r_s \sim 0.25 \text{ kpc}$  (also typical of SB nuclei) is then  $\sqrt{3} r_s / \lambda_{\text{pp}} \simeq 0.01$ . Thus, in a typical SB environment, characterized by relatively strong non-relativistic shocks ( $q_{\text{inj}} = 2.2$ ), the secondary to primary electron ratio is  $\chi = \chi_0 \sqrt{3} (r_s / \lambda_{\text{pp}}) \simeq 0.3$ . In a more quiescent environment, with typical values  $n_p \simeq 1 \text{ cm}^{-3}$  and  $r_s \sim 2.5 \text{ kpc}$ ,  $\chi \simeq 0.03$ . The higher value found in SBs is in approximate agreement with results of detailed numerical starburst models for energies  $\gtrsim 10 \text{ MeV}$  (plotted in, e.g., Paglione et al. 1996, Torres 2004, De Cea et al. 2009, Rephaeli et al. 2010).

To compute the p/e energy density,  $\kappa$ , we assume power-law spectra: (i) The electron spectral index  $q_e$  is deduced from the measured radio index  $\alpha$ , generally  $q_e = 2\alpha + 1$ . (ii) The proton spectral index is assumed to be close to the injection value,  $q_p \sim q_{\text{inj}} \simeq 2.1 - 2.2$ , for the dense SB environments hosted in the central regions of some galaxies, and equal to the leaky-box value,  $q_p = q_{\text{inj}} + \delta \simeq 2.7$  (where  $\delta \simeq 0.5$  is the diffusion index) for more quietly star forming galaxies.

Finally, we obtain an explicit expression for  $U_p$ :

$$U_p = \frac{1}{8\pi} \left[ 1 + \frac{1+\chi}{\kappa} \right]^{-1} \left[ \frac{7.44 \times 10^{-21}}{1+\chi} \left[ 1 + \frac{\kappa}{1+\chi} \right] \frac{\gamma_1^{2-q} 250^{q/2} \psi}{(q-2) a(q)} \right]^{\frac{4}{5+q}}. \quad (8)$$

Using Eq.(8), values of  $U_p$  can be obtained from the relevant observational quantities for our sample galaxies; these values are listed in Table 2. The quantities in Eq.(8) are usually well determined for our sample galaxies, except for the p/e energy density ratio  $\kappa$ , for which a spectral index,  $q_p$ , must be assumed. Given its possible values (i.e.,  $q_p \simeq 2.1 - 2.2$  in SB regions, and  $q_p \simeq 2.1 - 2.2$  for quiescent galaxies), the uncertainty in the spectral index,  $\delta q_p \simeq 0.1$ , translates to a factor of  $\sim 2$  uncertainty on  $\kappa$ , i.e. typically an uncertainty of  $\sim 50\%$  on  $U_p$  as deduced from Eq.(8).

### 3.2 Energetic particles and $\gamma$ -ray emission

Based on the calculation of  $\gamma$ -ray emission from SFGs outlined in Section 1,  $U_p$  can be estimated directly from recent measurements of the nearby galaxies. In SBGs, such as M82 and NGC 253, the central SB region (referred to also as the source

region) with a radius of  $\sim 200 - 300$  pc is identified as the main site of particle acceleration. The injected particle spectrum is assumed to have an index  $q = 2$ , the theoretically predicted  $N_p/N_e$  ratio is adopted, and equipartition is assumed. A measured radio index  $\alpha \simeq 0.7$  in the source region implies  $q = 2\alpha + 1 \simeq 2.4$  there, indicating a substantial steepening due to diffusion ( $D \propto \gamma^{-\delta}$ ), that cause the steady-state particle spectral index to be  $q_0 + \delta$  above some break energy. The procedure is similar when star formation does not (largely) occur in a burst in the nuclear region, but proceeds more more uniformly across the disk.

For a source with ambient gas number density  $n_{\text{gas}}$ , proton energy density  $U_p$ , and volume  $V$ , the integrated hadronic emission from  $pp$ -induced  $\pi^0$  decay is

$$L_{\geq E}^{[q]} = \int_V g_{\geq E}^{[q]} n_{\text{gas}} U_p dV \text{ s}^{-1}, \quad (9)$$

with the integral emissivity  $g_{\geq E}^{[\eta]}$  in units of  $\text{photon s}^{-1}(\text{H-atom})^{-1}(\text{eV/cm}^3)^{-1}$  (Drury et al. 1994). Thus,  $U_p$  can be determined from measurements of  $L_{\geq E}$  and  $n_{\text{gas}}(r)$ , and the particles steady-state energy distributions can be numerically calculated in the context of the convection-diffusion model.

In addition to the high-energy detections of the two local SBGs M82 and NGC 253 (Abdo et al. 2010a, Acciari et al. 2009; Acero et al. 2009), several galaxies with low SFR were also detected by the *Fermi* telescope. (i) the Andromeda galaxy M31 (Abdo et al. 2010b), with  $U_p \simeq 0.35 \text{ eV cm}^{-3}$ ; (ii) the Large Magellanic Cloud (LMC) whose average spectrum, either including or excluding the bright star-forming region of 30 Doradus, suggests  $U_p \simeq 0.2 - 0.3 \text{ eV cm}^{-3}$  (Abdo et al. 2010c); (iii) SMC for which  $U_p \simeq 0.15 \text{ eV cm}^{-3}$  was deduced (Abdo et al. 2010d). For the Milky Way, the modeling of the Galactic diffuse HE emission along the lines outlined above requires an average  $U_p \simeq 1 \text{ eV cm}^{-3}$  (Strong et al. 2010; Ackermann et al. 2011). Our values for  $U_p$  determined from the measured GeV-TeV fluxes are listed in Table 2.

### 3.3 Energetic particles and Supernovae

The SN origin of energetic particles suggested early on; as a test of this hypothesis, we estimate of  $U_p$  by combining the SN rate with the proton residence time,  $\tau_{\text{res}}$ , assuming a fiducial value for the fraction of SN kinetic energy that is channeled to particle acceleration. The residence time is determined from the p-p interaction time, and the two propagation timescales of advection and diffusion:

(i) The energy-loss timescale for  $pp$  interactions,  $\tau_{\text{pp}} = (\sigma_{\text{pp}} c n_p)^{-1}$ ; for protons with kinetic energy  $E \gtrsim 10$  TeV for which  $\sigma_{\text{pp}} \simeq 50$  mb, this timescale is

$$\tau_{\text{pp}} \simeq 2 \times 10^5 \left( \frac{n_p}{100 \text{ cm}^{-3}} \right)^{-1} \text{ yr}. \quad (10)$$

(ii) Particle advection out of the disk mid-plane region in a fast SB-driven wind occurs on a timescale  $\tau_{\text{adv}}$  determined from the advection velocity for which we adopt (except where noted otherwise) the nominal value  $v_{\text{adv}} \sim 1000 \text{ km s}^{-1}$ , deduced from measurements of the terminal outflow velocity of  $\sim 1600\text{-}2200 \text{ km s}^{-1}$  in M 82 (Strickland & Heckman 2009; see also Chevalier & Clegg 1985 and Seaquist & Odegard 1991). For a homogeneous distribution of SNe within the SB nucleus of radius  $r_s$ , the advection timescale is

$$\tau_{\text{adv}} \simeq 7.5 \times 10^4 \left( \frac{r_s}{0.3 \text{ kpc}} \right) \left( \frac{v_{\text{out}}}{1000 \text{ km s}^{-1}} \right)^{-1} \text{ yr}. \quad (11)$$

(iii) As noted in the previous section, diffusion is likely to be random walk against magnetic field inhomogeneities, with an estimated central diffusion coefficient,  $D \sim 3 \times 10^{28} \text{ cm}^2/\text{s}$ , assuming a magnetic coherence scale of  $\lambda \sim 1 \text{ pc}$ . Thus, diffusion out of the central 0.5 kpc is estimated to occur on a timescale

$$\tau_{\text{diff}} \simeq 3 \times 10^6 \left( \frac{r_s}{0.3 \text{ kpc}} \right)^2 \left( \frac{\lambda}{1 \text{ pc}} \right)^{-1} \text{ yr}. \quad (12)$$

Now, since the weighted residence time is

$$\tau_{\text{res}}^{-1} = \tau_{\text{pp}}^{-1} + \tau_{\text{adv}}^{-1} + \tau_{\text{diff}}^{-1}, \quad (13)$$

it is expected that - under typical conditions in central SB regions - p-p collisions and advection, more so than diffusion, effectively determine the survival there of energetic protons.

During  $\tau_{\text{res}}$ , the number of SN is  $v_{\text{SN}} \tau_{\text{res}}$ ; the kinetic energy deposited by each of these into the ISM is  $E_{\text{ej}} = 10^{51} \text{ erg}$  (Woosley & Weaver 1995). Arguments based on the energetic particle energy budget in the Galaxy and SN statistics suggest that a fraction  $\eta \sim 0.05 - 0.1$  of this energy is available for accelerating particles (e.g., Higdon et al. 1998). Thus, the proton energy density can be expressed as

$$U_p = 85 \left( \frac{v_{\text{SN}}}{0.3 \text{ yr}^{-1}} \right) \left( \frac{\tau_{\text{res}}}{3 \times 10^4 \text{ yr}} \right) \left( \frac{\eta}{0.05} \frac{E_{\text{ej}}}{10^{51} \text{ erg}} \right) \left( \frac{r_s}{0.3 \text{ kpc}} \right)^{-3} \text{ eV cm}^{-3}. \quad (14)$$

The resulting values of  $U_p$  in the sample galaxies are listed in Table 2.

## 4 Discussion

Detections of VHE  $\gamma$ -ray emission associated with ongoing star formation in M 82 and NGC 253 add significant new insight on the enhanced energetic electron and proton contents in SBGs, and on their propagation in disks of spiral galaxies. The common star-driven nature of NT phenomena in the wide class of non-AGN SFGs implies that energetic particle densities and radiation fields are self-similarly scaled

**Table 2** Star-forming galaxies: Proton energy densities<sup>+</sup>.

Object	$\gamma$ -ray meth.	radio meth.	SN meth.	other meth.	$r_s$ (kpc)	$\tau_{\text{res}}$ (yr)
Arp 220	–	1027	1142	–	0.25	2.0E+4
M 82	250 <sup>a,c</sup>	250	234	–	0.23	4.5E+4
NGC 253	220 <sup>b,c</sup>	230	213	–	0.20	6.7E+4
Milky Way	1 <sup>d</sup>	–	1.2	1 <sup>j</sup>	4.4	2.0E+7
	6 <sup>e</sup>	–	5	–	0.2	2.5E+6
M 31	0.36 <sup>f</sup>	0.22	0.7	–	4.5	2.5E+7
M 33	< 0.43 <sup>f</sup>	0.38	0.7	–	2.8	2.0E+7
LMC	0.21 – 0.31 <sup>g</sup>	0.22	0.4	–	2.5	4.4E+7
SMC	0.15 <sup>h</sup>	0.39	1.1	–	1.5	1.4E+7
NGC 4945	200 <sup>i</sup>	201	215	–	0.22	4.5E+4
NGC 1068	–	65	61	–	1.2	1.0E+6

<sup>+</sup> Values are in  $\text{eV cm}^{-3}$ .

(a) Acciari et al. (2009; see also Persic et al. 2008, De Cea et al. 2009). (b) Acero et al. (2009). (c) Abdo et al. (2010a). (d) Strong et al. (2010). (e) Aharonian et al. (2006). (f) Abdo et al. (2010b), and Drury et al. (1994) for M 33. (g) Abdo et al. (2010c). (h) Abdo et al. (2010d). (i) Lenain et al. (2010). (j) Webber (1987).

with SF activity, from quiescent systems to intense SBGs, in spite of the wide range of intrinsic physical conditions in these systems.

We have briefly outlined our treatment of the steady state spectro-spatial distributions of energetic electrons and protons in SFGs, exemplified in the case of the two nearby SBGs M 82 and NGC 253. This approach is based on a numerical solution of the diffusion-convection equation for particle distribution functions, following the evolution from the acceleration sites throughout the disk as the particles lose energy and propagate outward. Key observational normalization is based on measurements of radio synchrotron emission which, through an initial (theoretically assumed)  $N_p/N_e$  ratio provides also the normalization of the proton component. Assuming equipartition then allows to relate the local value of the mean magnetic field to the particle energy densities. The numerical solution of the diffusion-convection equation is based on an iterative procedure to determine the particle densities and mean field strength in the galactic center, and evolve these quantities by accounting for all relevant energy losses, and normalizing central values of these quantities by fitting to the measured radio spectrum from the central galactic (or SB) region. The quantitative viability of this approach is confirmed by the good agreement between the predicted high energy emission from M 82 and NGC 253 and measurements with *Fermi*, H.E.S.S., and VERITAS.

Significant detections of the NT emission from above two SBGs at lower (below 100 keV) X-ray energies, as would be expected by the currently operational NuSTAR telescope, will provide additional spectral coverage that will allow separating out the spectral electron and proton components. NuSTAR is the first X-ray telescope with capability to resolve this emission; if this is indeed achieved, important

new insight will be gained on the evolution of the electron spectro-spatial distribution across the disks of these nearby SBGs.

The three methods we have discussed to estimate energetic particle energy densities are clearly not independent. The  $\gamma$ -ray method and the radio method are coupled through the  $p/e$  ratio at injection, through the secondary-to-primary electron ratio, and through the imposed condition of particle-field equipartition. The SN method is not independent of the  $\gamma$ -ray method either, because both depend on the proton residence time, although - unlike the  $\gamma$ -ray and radio methods - it does not depend on the particle radiative yields but on the statistics of core-collapse SN. Also, the three methods do not stand on equal footing: with the  $\gamma$ -ray, radio, and SN methods we, respectively, either *measure*, *infer*, and or *estimate* the value of  $U_p$ . A substantial agreement among estimates based on the three methods is found for most of the galaxies in Table 1. The only exceptions are the SMC and NGC 1068. As for the former, the proton confinement volume could be small, so that most particles diffuse out to intergalactic space (Abdo et al. 2010d). If so, the  $\gamma$ -ray method yields the (lower) *actual* proton energy density, whereas the radio and SN methods estimate the (higher) *produced* amount. NGC 1068 hosts a prototypical Seyfert-2 nucleus (e.g., Wilson & Ulvestad 1982) surrounded by a spherical circumnuclear SB shell with external radius of 1.5 kpc and thickness 0.3 kpc, and mass  $3.4 \times 10^9 M_\odot$  (Spinoglio et al. 2005); its implied energy density is  $U_p \approx 65 \text{ eV cm}^{-3}$  from both the radio and SN methods. [We note that Lenain et al. (2010) suggested that the HE emissions of the above two SB and Sey II galaxies NGC 4945 and NGC 1068 are powered by, respectively, star formation and AGN activity.]

A debated aspect of proton energy loss and propagation times is whether the former is shorter than the latter; if so, the system is said to be a ‘proton calorimeter’ (e.g., Lacki et al. 2010, 2011). No galaxy in the above sample is found to be in the calorimetric limit; the two SBGs M 82 and NGC 253 would seem to be only marginally close to this limit. The presence of fast, SB-driven galactic winds advecting energetic particles out of the disk seems to be a ubiquitous feature in SBGs, limiting the degree at which they can be calorimetric. More generally, it is known that energetic particles do diffuse out of non-AGN SFGs, as evidenced also by significant radio emission (Ferrari et al. 2008), and possibly also high energy NT X-ray emission (Rephaeli et al. 2008) from large central regions of galaxy clusters. The estimated intracluster particle (and indeed also the magnetic) energy densities are sufficiently high, suggesting origin in the cluster galaxies.

Based on the reasonable hypothesis that local SB galaxies resemble young galaxies which were particularly abundant in the early universe, their contributions to the X- $\gamma$ -ray backgrounds are of obvious interest (e.g., Rephaeli et al. 1991). Calculations of the superposed emission from SBGs (Pavlidou & Fields 2002, Persic & Rephaeli 2003, Thompson et al. 2007, Fields et al. 2010, Lacki et al. 2011, Steckers & Venters 2011) indicate that this emission constitutes at least a tenth of these backgrounds.



## References

1. Abdo, A.A., et al. (LAT Collaboration) 2010a, *ApJL*, 709, L152
2. Abdo, A.A., et al. (LAT Collaboration) 2010b, *A&A*, 523, L2
3. Abdo, A.A., et al. (LAT Collaboration) 2010c, *A&A*, 512, A7
4. Abdo, A.A., et al. (LAT Collaboration) 2010d, *A&A*, 523, A46
5. Acciari, V.A., et al. (VERITAS Collaboration) 2009, *Nature*, 462, 770
6. Acero, F., et al. (HESS Collaboration) 2009, *Science*, 326, 1080
7. Ackermann, M., et al. (LAT Collaboration) 2012, *ApJ*, 755, 164
8. Ackermann, M., et al. (LAT Collaboration) 2011, *ApJ*, 726, 81
9. Aharonian, F., et al. (HESS Collaboration), 2006, *Nature*, 439, 695
10. Albert, J., et al. (MAGIC Collaboration) 2007, *ApJ*, 658, 245
11. Arieli, Y., & Rephaeli, Y. 2007, unpublished
12. Baltusaitis R.M., et al. 1984, *PRL*, 52, 1380
13. Beck R. 2000, in "The Interstellar Medium of M 31 and M 33", eds. E.M.Berkhuijsen, R.Beck, R.A.M.Walterbos (Aachen: Shaker), p.171 (astro-ph/0009455)
14. Beck, R., & Gräve, R. 1982, *A&A*, 105, 192
15. Bell, A.R. 1978, *MNRAS*, 182, 443
16. Carilli C.L. 1996, *A&A*, 305, 402
17. Chevalier, R.A., & Clegg, A.W. 1985, *Nature*, 317, 44
18. Corral P., Hollenbach D.J., Lord S.D., et al. 1994, *ApJ*, 423, 223
19. Cox D.P. 2005, *ARA&A*, 43, 337
20. de Cea Del Pozo, E., Torres, D.F., & Rodriguez Marrero, A.Y. 2009, *ApJ*, 698, 1054
21. Diehl R., Halloin H., Kretschmer K., et al., 2006, *Nature*, 439, 45
22. Domingo-Santamaría, E., & Torres, D.F. 2005, *A&A*, 444, 403
23. Drury, L.O'.C., Aharonian, F.A., & Völk, H.J. 1994, *A&A*, 287, 959
24. Elmouttie M., Haynes R.F., Jones, K.L., et al. 1997, *MNRAS*, 284, 830
25. Enomoto, R., et al. 2008, *ApJ*, 683, 383
26. Ferrari, C. Govoni, F., Schindler, S., Bykov, A., & Rephaeli, Y. 2008, *Space Science Reviews*, 134, 93
27. Fields, B.D., Pavlidou, V., & Prodanovic, T. 2010, *ApJ*, 722, L199
28. Goldshmidt, O., & Rephaeli, Y. 1995, *ApJ*, 444, 113
29. Haynes, R.F., Klein, U., Wayte, S.R., et al. 1991, *A&A*, 252, 475
30. Heesen, V., Beck, R., Krause, M., Dettmar, R.J. 2008, *A&A*, 494, 563
31. Helou G., Khan I.R., Malek L., Boehmer L. 1988, *ApJS*, 68, 151
32. Higdon, J.C., Lingenfelter, R.E., & Ramaty, R. 1998, *ApJ*, 509, L33
33. Kennicutt, R.C. Jr. 1998, *ARAA*, 36, 189
34. Kewley L.J., Heisler C.A., Dopita M.A., et al. 2000, *ApJ*, 530, 704
35. Klein, U., Wielebinski, R., Haynes, R.F., & Malin, D.F. 1989, *A&A*, 211, 280
36. Klein U. et al. 1983, *Å127*, 177
37. Kühr H., Witzel A., Pauliny-Toth I.I.K., Nauber U. 1981, *A&AS*, 45, 367
38. Lacki, B.C., Thompson, T.A., & Qataert, E. 2010, *ApJ*, 717, 1
39. Lacki, B.C., Thompson, T.A., Quataert, E., Loeb, A., & Waxman, E. 2011, *ApJ*, 734, 107
40. Lenain J.-P., Ricci C., Türler M., Dorner D., Walter R. 2010, *A&A*, 524, 72L
41. Lerche, I., & Schlickeiser, R. 1982, *MNRAS*, 201, 1041
42. Mannucci F., Maiolino R., Cresci G., et al. 2003, *A&A*, 401, 519
43. Moorwood A.F.M. & Oliva E. 1994, *Apj*, 429, 602
44. Moskalenko I.V., & Strong A.W. 1998, *ApJ*, 493, 694
45. Moskalenko I.V., Jones, F.C., Mashnik, S.G., Ptuskin, V.S., & Strong, A.W., 2003, *ICRC*, 4, 1925
46. Paglione, T.A.D., Marscher, A.P., Jackson, J.M., & Bertsch, D.L. 1996, *ApJ*, 460, 295
47. Pavlidou, V., & Fields, B.D. 2001, *ApJ*, 558, 63
48. Pavlidou, V., & Fields, B.D. 2002, *ApJ*, 575, L5
49. Persic, M., & Rephaeli, Y. 2003, *A&A*, 399, 9



50. Persic, M., & Rephaeli, Y. 2010, MNRAS, 403, 1569
51. Persic, M., & Rephaeli, Y. 2012, in preparation
52. Persic, M., Rephaeli, Y., & Arieli, Y. 2008, A&A, 486, 143 (PRA)
53. Petuchowski SJ, Bennett CL, Haas MR, et al. 1994, ApJ, 427, L17
54. Points S.D., Chu Y.-H., Snowden S.L., Smith R.C. 2001, ApJS, 136, 99
55. Protheroe, R.J., & Clay, R.W. 2004, PASA, 21, 1
56. Rephaeli, Y. 1988, Comm. Ap., 12, 265
57. Rephaeli, Y. 1979, ApJ, 227, 364
58. Rephaeli, Y., Arieli, Y., & Persic, M 2010, MNRAS, 401, 473
59. Rephaeli, Y., Gruber, D.E., Persic, M., & MacDonald, D. 1991, ApJ, 380, L59
60. Rephaeli, Y., Nevalainen, J., Ohashi, T., & Bykov, A. 2008, Space Science Reviews, 134, 71
61. Romero, G.E., & Torres, D.F. 2003, ApJ, 586, 33
62. Roy A.L., Oosterloo T., Goss W.M., Anantharamaiah K.R. 2010, A&A, 517, A82
63. Sasaki, M., Haberl, F., & Pietsch, W. 2002, A&A, 392, 103
64. Schlickeiser, R. 2002, Cosmic Ray Astrophysics (Berlin: Springer), p.472
65. Seaquist, E.R., & Odegard, N. 1991, ApJ, 369, 320
66. Spinoglio L., Malkan M.A., Smith H.A., et al. 2005, ApJ, 623, 123
67. Spoon H.W.W., Koornneef J., Moorwood A.F.M., Lutz D., Tielens A.G.G.M. 2000, A&A, 357, 3000
68. Stecker, F.W., & Venters, T.M. 2011, ApJ, 736, 40
69. Strickland, D.K., & Heckman, T.M. 2009, ApJ, 697, 2030
70. Strickland et al. 2002, ApJ, 568, 689
71. Strickland, D.K., Ponman, T.J., & Stevens, I.R. 1997, A&A, 320, 378
72. Strong, A.W., Porter, T.A., Digel, S.W., et al. 2010, ApJ, 722, L58
73. Tabatabaei F.S., Beck R., Krügel E., et al. 2007, A&A, 475, 133
74. Tabatabaei F.S., Krause M., Fletcher A., Beck R. 2008, A&A, 490, 1005
75. Thompson, T.A., Quataert, E., Waxman, E. 2007, ApJ, 654, 259
76. Torres, D.F. 2004, ApJ, 617, 966
77. Torres, D.F., Cillis, A., Lacki, B., & Rephaeli, Y. 2012, MNRAS, 423, 822
78. Tucker, W. 1975, *Radiation Processes in Astrophysics* (Cambridge, MA: MIT Press)
79. Ulvestad 2000, AJ, 120, 278
80. van den Bergh, S., & Tammann, G.A. 1991, ARAA, 29, 363
81. Webber, W.R. 1987, A&A, 179, 277
82. Weinberg, M.D., & Nikolaev, S. 2001, ApJ, 548, 712
83. Wilke, K., Stickel, M., Haas, M., et al. 2003, A&A, 401, 873
84. Wilson, A.S., & Ulvestad, J.S., 1982, ApJ, 263, 576
85. Woosley, S.E., & Weaver, T.A. 1995, ApJS, 101, 181
86. Zirakashvili, V.N., Breitschwerdt, D., Ptuskin, V.S., & Voelk, H.J. 1996, A&A, 311, 113